

Assessing the impact of urban geometry on surface urban heat island using complete and nadir temperatures

Jinxin Yang¹ | Massimo Menenti^{2,3} | Zhifeng Wu^{1,4} | Man Sing Wong⁵ |
 Sawaid Abbas⁵ | Yong Xu¹ | Qian Shi⁶

¹School of Geography and Remote Sensing, Guangzhou University, Guangzhou, 510006, China

²Faculty of Civil Engineering and Earth Sciences, Delft University of Technology, P. O. Box 5048, 2600, Delft, Netherlands

³State Key Laboratory of Remote Sensing Science, Institute of Remote Sensing and Digital Earth, Chinese Academy of Sciences, Beijing, 100101, China

⁴Southern Marine Science and Engineering Guangdong Laboratory, Guangzhou, 511458, China

⁵Department of Land Surveying and Geo-Informatics, The Hong Kong Polytechnic University, Kowloon, Hong Kong

⁶School of Geography and Planning, Sun Yat-sen University, Guangzhou, 510275, China

Correspondence

Zhifeng Wu, School of Geography and Remote Sensing, Guangzhou University, Guangzhou 510006, China.
 Email: zfwu@gzhu.edu.cn

Funding information

Guangdong Provincial Natural Science Foundation, Grant/Award Number: 2018B030312004; National Natural Science Foundation of China, Grant/Award Numbers: 41901283, 61976234; State Administration of Foreign Experts Affairs, Grant/Award Number: G20190161018; the Hong Kong Research Grants Council, Grant/Award Number: 15602619; the Junta de Andalucía, Grant/Award Number: P10-TIC-6114

Abstract

The surface urban heat island intensity (SUHII) when using nadir-viewing radiometric and complete surface temperature (T_r and T_c) was evaluated. The urban areas of the Kowloon peninsula and Hong Kong Island were selected and four daytime Landsat TM images and two nighttime ASTER images were collected to retrieve T_r and then model T_c based on a semi-empirical model. SUHIIc were estimated using both the retrieved T_r and modelled T_c . High spatial resolution (HR) airborne thermal images (0.2 m) observed at 12:10 noon on Oct 24, 2017 were used to retrieve T_c directly. Results based on HR data and satellite data were consistent and indicated that the geometry of the built-up space had a larger impact on SUHII when using T_c (SUHIIc) than T_r (SUHIIr). During daytime SUHIIc decreased while SUHIIr showed a very slight increase with building density. Both SUHIIc and SUHIIr decreased with higher building height but the rate of decrease of SUHIIc was higher than SUHIIr. Both SUHIIc and SUHIIr decreased with increasing building height variance and increased with increasing sky view factor (SVF). The rate of decrease with building height variance for SUHIIc was larger than SUHIIr. The rate of increase of SUHIIc with SVF was higher than SUHIIr. During nighttime, geometry effects on SUHIIc and SUHIIr were different from daytime. Both SUHIIc and SUHIIr increased with building density, while the rate of increase of SUHIIc with building density, as well as with building height, was much higher than SUHIIr. Both SUHIIc and SUHIIr decreased with SVF, but the rate of decrease of SUHIIc was higher than SUHIIr. Both SUHIIc and SUHIIr initially increased with building height variance and then remained

Abbreviations: SUHIIc, The difference between the complete surface temperature of reference rural areas and the complete surface temperature of urban areas; SUHIIr, The difference between the radiometric surface temperature of reference rural areas and the radiometric surface temperature of urban areas; UHII, The difference between air temperature of reference rural station and the air temperature of urban stations.

approximately constant. We also evaluated the UHI intensity: SUHIIc was much closer to UHII than SUHIIr. Overall, building geometry had larger impact on SUHIIc than on SUHIIr, that is, SUHIIc is more representative of urban climate than SUHIIr.

KEY WORDS

surface urban heat island, thermal remote sensing, urban geometry

1 | INTRODUCTION

Urbanization leads to the replacement of bare soil and vegetation by impervious surfaces, which reduces the potential for mitigation of ambient temperature through evaporation and transpiration (Oke, 1982; Oke *et al.*, 1989; Shahmohamadi *et al.*, 2010; Kuang *et al.*, 2015). Instead, the radiative energy absorbed by the built-up space has to be dissipated mainly as sensible heat flux in addition to the release of anthropogenic heat, warming the surface and the atmosphere (Oke, 1981; Oke *et al.*, 1999). This makes the urban air and surface temperature higher than the rural surface temperature because more abundant vegetation in rural areas dissipates more energy through evaporation and transpiration, thus cooling both the air and the land surface. This then has an impact on the value of both the urban heat island (UHI) and surface urban heat island (SUHI) indicators of urban climate. Both UHI and SUHI have several impacts on urban climate and residents, including increasing the energy consumption for space cooling and heat stress on human residents in summer (Oke *et al.*, 2017).

The UHI metrics apply air temperature measured in the urban canopy below roof-level in the urban canyons and use rural meteorological stations as a reference (Oke, 1981; Stewart, 2011). SUHI is defined as the difference between urban surface temperature at any urban location and the surface temperature of reference rural areas (Roth *et al.*, 1989; Stewart, 2011). Differences between the urban and rural areas in the relative magnitude of radiative and convective flux densities at the land – atmosphere interface result in different air and surface temperature in urban and rural areas, thus UHI and SUHI are indicators of the difference in surface energy balance between urban and rural areas. In other words, both UHI and SUHI are indicators of the overall effect of the built-up space on the surface energy balance.

Air and surface temperatures are different geophysical variables in many ways (Oke *et al.*, 2017), and air temperature is measured at meteorological stations that often have spatial densities insufficient to characterize urban

scale variability. The development of thermal infrared remote sensing made available spatially continuous observations of the land surface temperature across a range of spatial resolutions and the SUHI is based on spatially detailed observations of the radiometric surface temperature captured by space- and airborne imaging radiometers (Zhou *et al.*, 2018). Such spatially continuous data provide detailed information towards a better understanding of urban climate and its drivers. The dependence of SUHI on the urban land cover has been studied often (Weng *et al.*, 2004; Chen *et al.*, 2006; Yuan and Bauer, 2007; Li *et al.*, 2016). Recently, the dependence of SUHI on the geometry of the urban built-up space has also been addressed (Yu *et al.*, 2019). The impact of shadows determined by urban geometry has been studied by Yu *et al.* (2019) and results showed that in Beijing the building shadow reduced by 3.16 K the temperature of the urban impervious surface in July. More generally, the effect of urban morphology on radiometric surface temperature has been studied by Huang and Wang (2019) and the results showed that the urban geometric parameters have complex effects on the 2D and 3D pattern in urban radiometric surface temperature provided by Landsat thermal images. The urban thermal heterogeneity and 3D geometry, combined with the observation direction, lead to changes in directional radiometric temperature with view angle that is, thermal anisotropy (Oke *et al.*, 2017). Studies from Toulouse city centre show the thermal anisotropy can reach 10 K on clear summer days (Lagouarde *et al.*, 2010; Lagouarde *et al.*, 2012). This severely affects mapping of radiometric surface temperature and then the interpretation of SUHI (Voogt, 2011; Zhan *et al.*, 2012; Hu and Brunsell, 2013; Huang *et al.*, 2016; Wang *et al.*, 2018; Wang and Chen, 2019; Li and Li, 2020). Current studies on SUHI are based on the radiometric surface temperature observed by thermal imaging radiometers above the urban canopy without considering the impact of anisotropy (Weng *et al.*, 2004; Peng *et al.*, 2012; Li *et al.*, 2016). The radiometric surface temperature is mainly related to horizontal facets, for example, roof and road, because most imaging radiometers are designed for nadir or near nadir looking (Roth *et al.*, 1989; Voogt and Oke, 2003; Zhou *et al.*, 2019).

The impact of urban geometry on the application of thermal infrared remote sensing for urban climate research was highlighted by Roth *et al.* (1989) and then further clarified and studied systematically by Voogt and Oke (1997, 1998, 2003). Roth *et al.* (1989) focused on SUHI evaluated on average for a large, mixed urbanized area using low resolution AVHRR data and discussed the limitation of the application of thermal remote sensing to study urban climate. Voogt and Oke (1997) introduced the complete surface temperature and evaluated the impact of observation geometry on measured surface temperature. Voogt and Oke (1998) documented the impact of anisotropy on the thermal infrared exitance of selected urban targets and the surface brightness temperature retrieved from data acquired by an airborne imaging radiometer. Voogt and Oke (2003) reviewed the state of the art of thermal infrared remote sensing of urban landscapes. These studies document the notion that the complete surface temperature, which captures all the facet temperatures, is a more meaningful variable for urban climate research, since it includes information on all facets.

Different facets of the urban surface contribute to meteorological processes differently, and all facets of the urban surface area are involved in the urban land surface processes and energy exchange and should be considered. The experiment conducted in Hong Kong by Ng *et al.* (2012) showed that a green roof is ineffective to improve thermal comfort at ground level, while trees at street level are effective in cooling pedestrian areas. This means that a roof top facet may not affect the urban canopy layer air temperature near the ground, while the wall or road or other near ground facets would do so. Thus, the complete surface temperature is useful to study urban climate since it provides the information required for urban climate research, for example, to estimate sensible heat flux (Voogt and Grimmond, 2000; Yang *et al.*, 2019) and other heat flux densities.

SUHI is an important micro-climate indicator in urban areas. The complete surface temperature may be more useful than the radiometric surface temperature to map SUHI intensity, but it has been rarely used. The difference between complete and radiometric surface temperature can reach 10 K (Voogt and Oke, 1997; Allen *et al.*, 2018; Jiang *et al.*, 2018). This would lead to large differences between SUHI maps generated with either surface temperature. Thus, this study is based on the theoretical knowledge of urban geometry, and it applies thermal infrared image data and complete surface temperature (Roth *et al.*, 1989; Voogt and Oke, 1997; Voogt and Oke, 2003) to map and compare SUHIs evaluated with radiometric and (estimated) complete urban surface temperatures.

In order to explore the differences in SUHIs when using different surface temperatures, this study will investigate the dependence of SUHIs on urban geometric structure when using either the complete or radiometric surface temperatures towards a better understanding of the information encapsulated in SUHI.

2 | METHODOLOGY

In order to study the impact of geometry on different SUHIs, satellite data acquired by the Landsat 5 (L5) / Thematic Map (TM) (30 m x 30 m after resampling) and the Advanced Spaceborne Thermal Emission and Reflection Radiometer (ASTER) (90 m x 90 m) and the airborne high-spatial resolution (0.2 m x 0.2 m) thermal data were collected. The satellite data of Landsat TM and ASTER were used to retrieve the radiometric surface temperature using the single channel method (Equation 1) (Yang *et al.*, 2015) and then estimate the T_c by applying the method developed by (Yang *et al.*, 2020a) (Equation 2 and Equation 3):

$$E(i) = \tau_i \left[\epsilon(i)B(T_r(i)) + (1 - \epsilon(i))R_{at}^\downarrow(i) \right] + R_{at}^\uparrow(i) \quad (1)$$

$E(i)$ is the radiance received by a radiometer at the top of atmosphere of pixel i . τ_i is the effective transmittance of the atmosphere, $R_{at}^\uparrow(i)$ is the upwelling and $R_{at}^\downarrow(i)$ is the downwelling atmospheric radiance. In the thermal band of L5 / TM current values of these atmospheric parameters can be obtained from the NASA Atmospheric Correction Parameter Calculator (<http://atmcorr.gsfc.nasa.gov/>). The radiance of ASTER AST 09 T product used in this study is the ground-leaving in-band radiance including the emission of surface, the reflected radiance by the surface $[\epsilon(i)B(T_r(i)) + (1 - \epsilon(i))R_{at}^\downarrow(i)]$ and the sky thermal irradiance in band 13 of the ASTER AST 09 T product can be used to calculate the downwelling radiance to retrieve the urban radiometric surface temperature (Sobrino *et al.*, 2007). $\epsilon(i)$ is the material emissivity of pixel i , estimated as the area-weighted average of the material emissivity of component horizontal facets, for example, roofs, roads and ground, within the footprint observed by a nadir viewing imaging radiometer (see Yang *et al.* (2016b) for details). $B(T_r(i))$ is the upwelling radiance of pixel i with radiometric temperature $T_r(i)$. $T_r(i)$ can be derived from $B(T_r(i))$ based on the Planck function.

The radiometric surface temperature (T_r) observed by a nadir or near-nadir viewing remote sensor over an urban canopy includes the emitted and reflected radiance from horizontal surfaces. The reflected radiance from

horizontal surfaces includes a contribution from the radiance emitted by vertical surfaces that are not directly observed by nadir or near-nadir viewing remote sensors. The urban geometry causes the difference between T_r and the complete surface temperature (T_c) and material heterogeneity enhanced by local meteorological conditions. Yang et al., (2020a) employed an urban microclimate model – the Temperatures of Urban Facets in 3-D (TUF-3D) model – to estimate T_c from modelled T_r generated by numerical experiments. The TUF-3D model has been evaluated under different neighbourhood and climate conditions (Krayenhoff and Voogt, 2007; Crawford et al., 2018) and has been used to evaluate radiation models (Krayenhoff et al. 2014) and to provide surface temperatures for remote sensing research (Krayenhoff and Voogt, 2016; Wang et al., 2020).

According to Yang et al. (2020a), the relationships between T_c and T_r can be written as:

For daytime,

$$T_c(i) = 0.913 * T_r(i) - 5.390 * \lambda_p(i) - 1.090 * \ln(F(i)) + 0.001 * Kn(i) - 0.013 * \theta_a(i) + 0.139 * \theta_z(i) + 20.598, \text{ with } r^2 = 0.97, \text{ RMSE} = 1.500 \text{ K} \quad (2)$$

For nighttime,

$$T_c(i) = 0.927 * T_r(i) + 3.455 * \lambda_p(i) + 0.184 * \ln(F(i)) + 21.320, \text{ with } r^2 = 0.98, \text{ RMSE} = 0.690 \text{ K} \quad (3)$$

$T_r(i)$ is the nadir-view radiometric surface temperature estimated according to Equation (1), which also takes into account the geometry of the built-up space within the footprint of the radiometer, but captures the exitance of horizontal facets only, $\lambda_p(i)$ is building density, $F(i)$ is the wall area index, calculated as the ratio of wall area to horizontal area, $Kn(i)$ is the solar irradiance onto the urban canopy (Wm^{-2}), $\theta_a(i)$ is solar azimuth angle ($^\circ$), $\theta_z(i)$ is solar zenith angle ($^\circ$). These parameters were selected because they are the main factors that affect the difference between T_c and T_r , after evaluation of the simulated data mentioned above (Yang et al., 2020a).

The method developed to estimate the complete surface temperature by Yang et al. (2020a) (Equation 2 and Equation 3) was evaluated using a synthetic, model-based data set, and results showed it can reach good accuracy ($r^2 = 0.97$, RMSE = 1.500 K for daytime and $r^2 = 0.98$, RMSE = 0.690 K for nighttime). The relationships suggested by Yang et al. (2020a) were developed using simulated data by carrying out a large number of numerical experiments with TUF – 3D for a wide range of key model parameters and atmospheric forcing variables. The method of Yang et al. (2020a), therefore, is not

limited to the specific conditions applying to the image data used to evaluate and demonstrate the approach.

The method to estimate the complete surface temperature developed by Yang et al. (2020a) is only applicable to urban areas with no or sparse vegetation cover, thus we only analysed the impact of urban geometry on SUHIIIs in built-up areas without vegetation. The impact of vegetation fractional cover and structure on SUHIIIs will not be analysed in this study. This study will only focus on the impacts of building geometric parameters on SUHIIIs, for example, building height, building density, Sky View Factor (SVF) and building height difference. The building density is calculated as the ratio of roof area to a lot area. The SVF is calculated for all horizontal surfaces including roofs and ground. The ratio of the roof to complete area and spacing of buildings may also have an impact on the relation of SUHIIr with SUHIIc. The building density, height and SVF can account for the effects of these parameters. Thus, this study chose building density, building height, SVF and building height deviation to evaluate the relation between SUHII-s and urban geometry.

The usage of T_c estimated from T_r , retrieved from TOA radiometric data acquired by space-borne imaging radiometers, is attractive because of the spatial and temporal coverage, although the spatial resolution of current observation systems is not sufficient to capture the urban landscape with sufficient detail. On the other hand, it needs to be evaluated whether the estimated T_c correctly captures the effect of urban geometry on the urban surface temperature. To this end, we have applied thermal infrared observations at 0.2 m x 0.2 m spatial resolution to determine directly T_c . A helicopter-mounted thermal camera acquired these observations and flight lines were in different directions to acquire multiple observations of the same target under different view angles (Figure 1). These data allowed the direct determination of T_c for a large number of urban facets. The atmospheric and emissivity correction were conducted first by applying the thermal image process software ResearchIR provided by the Flir company (<https://www.flir.cn/>). The information on different facets can be obtained from different view directions (Figure 1). The HR data were gridded at 100 m x 100 m to calculate the T_c within each grid, with T_r being the temperature observed at nadir or near-nadir direction. We visually identified each facet in the grid to estimate T_c as the area-weighted mean temperature of facets observed under different directions.

We have evaluated the two retrievals of T_c by analysing the dependence of both retrievals on urban geometry. The relationship between SUHIIc and the urban geometry parameters was evaluated twice, that is, using both the T_c estimated from T_r (satellite retrievals) and the

FIGURE 1 The HR images observed from different directions: (a), front direction; (b), left direction; (c), near nadir direction; (d), right direction; (e), back direction

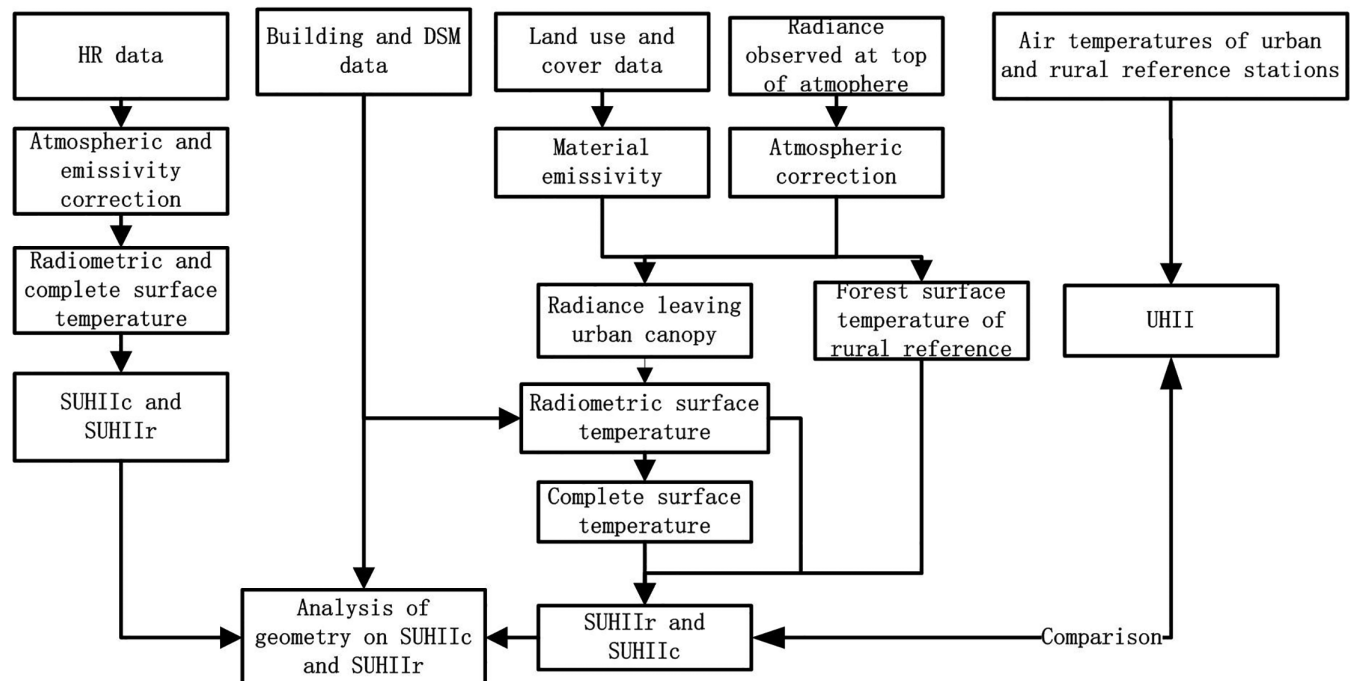
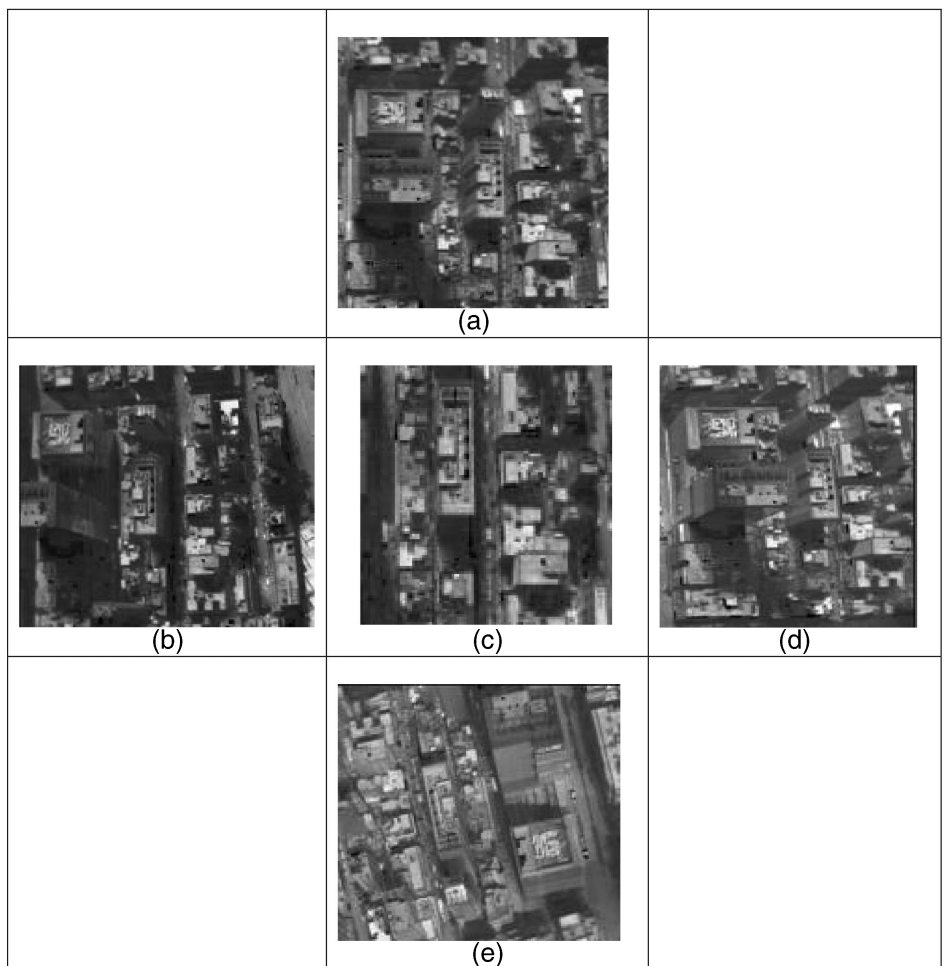


FIGURE 2 Flow chart of this study

TABLE 1 Metrics applied in this study to evaluate the urban heat island effect

Abbreviations	Calculation methods
SUHIIc	The difference between the surface temperature of reference rural areas and the pixel-wise complete surface temperature of urban areas
SUHIIr	The difference between surface temperature of reference rural areas and the nadir-viewed radiometric surface temperature of urban areas
UHII	The difference between air temperature of reference rural station and the air temperature of urban stations

T_c determined with the high resolution thermal infrared data. This objective of the evaluation was to provide insights on the impact of the two procedures to retrieve T_c on the assessment and interpretation of SUHIIc and of its dependence on urban geometry.

UHI intensity (UHII) is calculated using the air temperature observed by meteorological stations in rural and urban areas and compared with the SUHIIc based on urban radiometric and complete surface temperature. The UHII cannot be resolved with much spatial detail in this study since only a few observation stations are available, namely the three urban meteorological stations at Hong Kong Observatory (HKO), King's Park (KP) and Sham Shui Po (SSP) (Figure 2). The mean values of SUHIIc within a 250 m buffer zone around the three urban stations will be compared with UHIIc as suggested by (Yang *et al.*, 2020b), since the highest correlation coefficient between building and air temperature was obtained when averaging the SUHIIc-s within such 250 m buffer zone. The definitions of different urban heat island metrics are summarized in Table 1. The flowchart of this study is shown in Figure 2.

3 | RESEARCH AREA AND DATA

Urban districts of the Kowloon peninsula and Hong Kong Island across Hong Kong were selected as our study area (Figure 3). In brief, Hong Kong is a coastal city in South China ($22^{\circ} 17' N$, $114^{\circ} 09' E$), and this study area has been recognized as a compact city with high-density built-up space (Chen *et al.*, 2012). Due to this high-rise, high-density urban environment, urban canyons have formed that influence microclimate significantly (Chen *et al.*, 2012). In this condition, the effect of urban geometry on SUHI is complex. The observed radiometric surface temperature cannot represent the real urban

surface temperature in such a compact city. Thus, the SUHI based on T_c should be explored for urban climate research in Hong Kong. According to Siu and Hart (2013), the Tsak Yue Wu station (TYW) ($22.40278 N, 114.32306 E$) is regarded as a representative rural station because it is surrounded by forest and far away from the sea, thus was used as a reference to determine both UHI and SUHIIc. The three urban stations are at the center of the urban area and sufficiently far from the sea for the airflow to adjust to the temperature in the urban area before reaching the stations, regardless of the direction. Thus, the impact of sea breeze on the UHII pattern can be neglected. The surface temperature within the 250 m buffer around the Tsak Yue Wu station was taken as the rural surface reference to calculate the SUHIIc.

The radiometric temperatures retrieved from L5 / TM data in 2010 to 2011 (2010, March 26; 2010, Sep 18; 2010, December 23; 2011, June 1) and ASTER in 2013 (2013, Mar 13; 2013, Aug 4) were used in this study. Table 2 shows the observation time and dates of satellite data used in this study. Figure 4 shows the satellite radiometric and complete surface temperature data used in this study and the retrieval method and accuracy have been described in detail by (Yang *et al.*, 2020a). The HR thermal images of a part of the urban area of Kowloon peninsula at noontime (12:10) of Oct 24, 2017 (Figure 5) were collected to estimate the T_c and Tr. This area was gridded into 120 cells for further analysis. The air temperatures observed by meteorological stations in urban and rural areas at the time of the acquisition of satellite data were collected to calculate the UHII. The building data and DSM data derived by LiDAR with 1 m spatial resolution were collected to provide the building height, building height difference, building density, and sky view factor. The building height, density, building height and the sky view factor are shown in Figure 6 and described in detail by (Yang *et al.*, 2015).

4 | RESULTS

4.1 | Evaluation of different SUHIIc

4.1.1 | SUHIIc from satellite data

The forest surface temperature at TYW after topographic correction was applied as a reference temperature to calculate the SUHIIc (Figure 7). The SUHIIc based on radiometric surface temperature (SUHIIr) is much higher than the SUHIIc based on complete surface temperature (SUHIIc). The difference between SUHIIr and SUHIIc varies with building geometric conditions. In winter the

FIGURE 3 Study area of this study: Red box in b is for c; blue box in b is for d

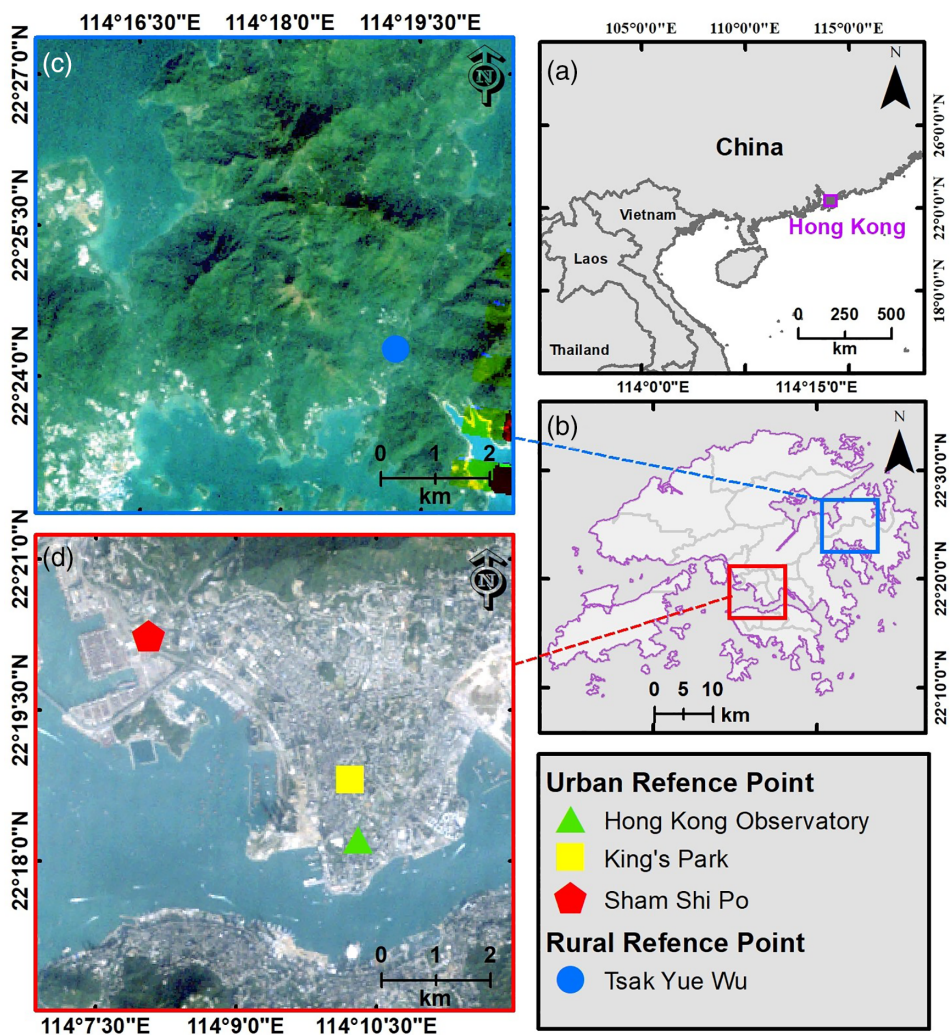


TABLE 2 Satellite data used in this study

Satellite	Date	Local time
Landsat 5	March 26, 2010	10:43
	September 18, 2010	10:42
	December 23, 2010	10:42
	June 1, 2011	10:41
ASTER	March 13, 2013	22:36
ASTER	August 4, 2013	22:36

difference between SUHIIr and SUHIIc in built-up areas can reach 7.5 K and the mean difference was 3.70 K with a standard deviation of 2.21 K when determined with the data observed by Landsat TM on Dec 23, 2010. In summer, this difference can reach 12.00 K while the mean difference was 8.00 K with a standard deviation of 3.32 K when determined with the data observed by Landsat TM on Jun 1, 2011. The SUHIIc can even show a cool island

phenomenon, that is, $[T_c(\text{urban}) < T_c(\text{rural})]$. Generally, the latter appeared in the areas with dense buildings. The dominant factor of urban climate in daytime is solar radiation and the shadow and blockage by the buildings reduce irradiance thus reduces the surface temperature within the urban canopy. The roof and street surface temperature mainly determine the radiometric temperature. The high exposure of the roof surface to solar radiation helps make the roofs surface temperature much higher than wall and street. This makes the SUHIIr much higher than SUHIIc. The building shadows make the wall and street facets cooler and people may feel cooler than in rural areas without shading. This shading, combined with the thermal properties of urban materials, can result in a cool urban island. Nadir-view radiometric temperatures, with their biased view of hotter surfaces such as roofs, are less likely to capture this effect, thus the SUHII based on T_r may not detect this effect. The SUHII value is heavily affected by the selection of the rural reference, that is, choosing a rural station with bare soil instead of

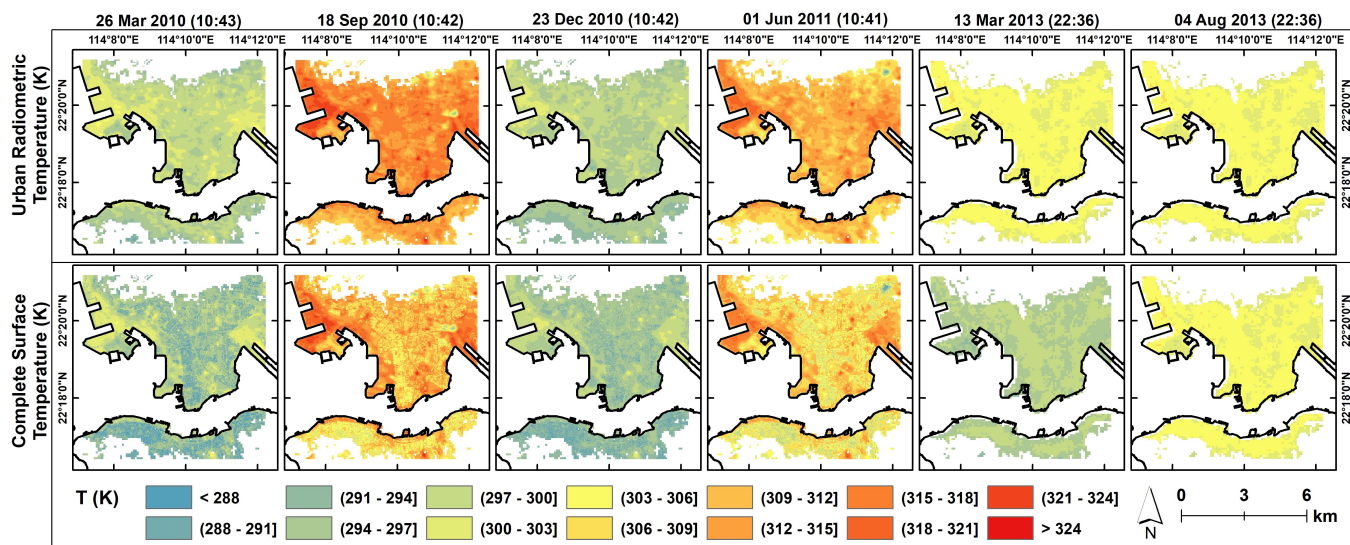


FIGURE 4 Satellite nadir and complete surface temperatures used in this study

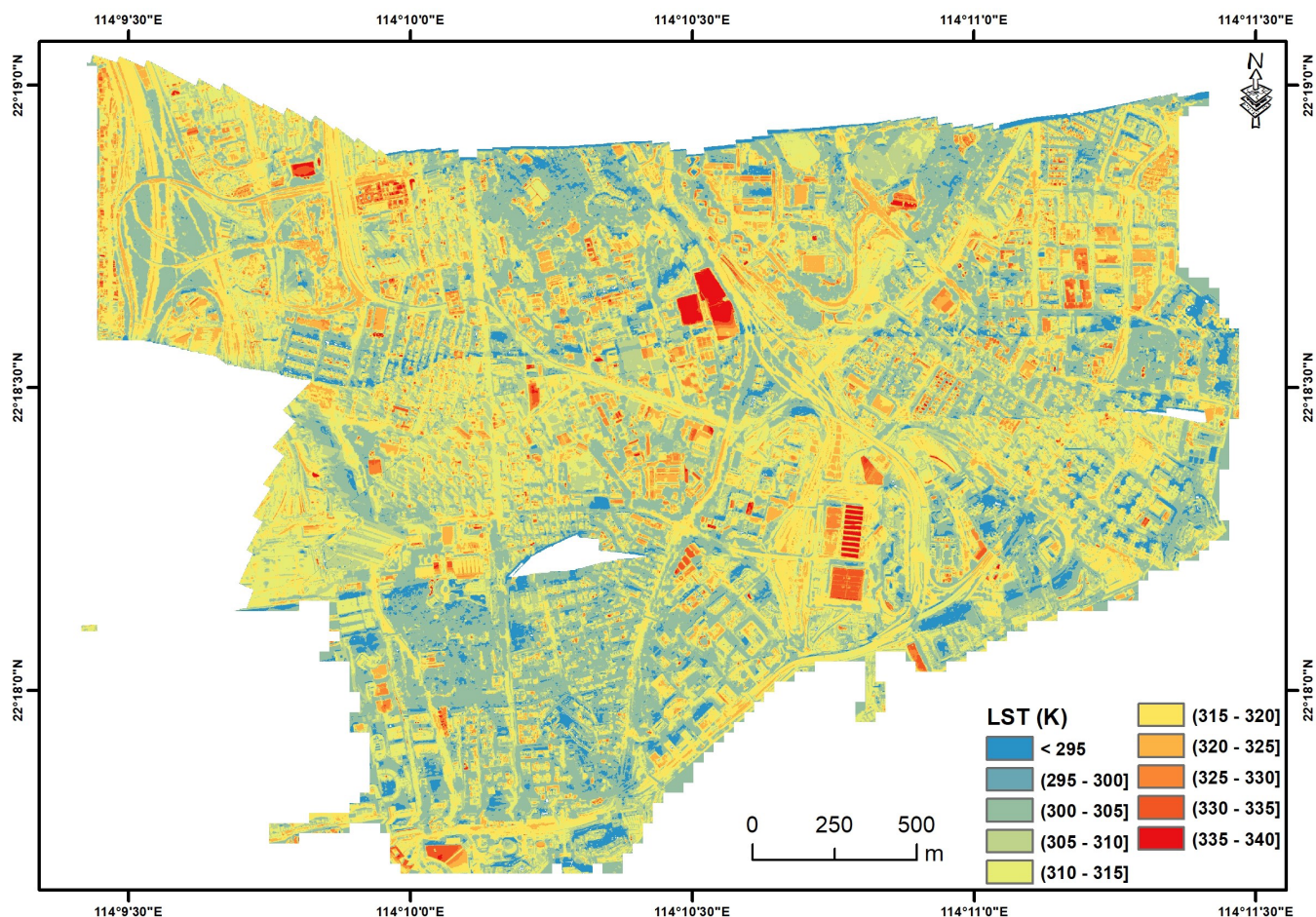
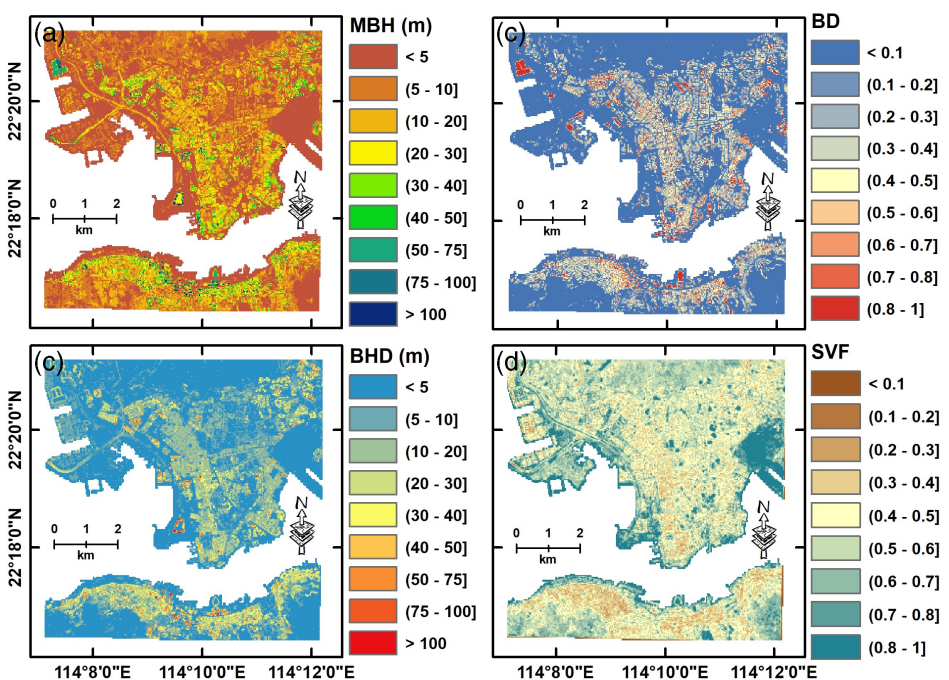


FIGURE 5 High resolution nadir thermal image observed at 12:10 of Oct 24, 2017

FIGURE 6 A, building mean height; b, building density; c, building height deviation; d, SVF



vegetation as a reference, the urban cool islands may also be observed by nadir-view radiometers (Carnahan and Larson, 1990).

The surface urban cool island conditions do not appear in night time (Figure 8), since the longwave radiative and convective exchange within the urban space is the dominant factor. The urban surface releases energy to the atmosphere in night time by longwave emission and by convective fluxes. The atmospheric longwave radiation absorbed by the land surface during nighttime is smaller than solar irradiance during daytime, when solar irradiance is the dominant factor. The shaded facets enhance the difference between T_c and T_r during daytime. Thus, the difference between SUHIr and SUHIIc during nighttime is much smaller than that in daytime. The maximum difference is only about 2.00 K and the mean difference was 0.60 K on March 13th, 2013, while the maximum difference was only about 1.50 K and the average was about 0.10 K on August 4th, 2013. Thus, the surface urban cool island based on complete surface temperature only appears in daytime and this is similar to the UHI based on air temperature.

4.1.2 | SUHIIs from HR thermal data

The HR thermal images do not provide the surface temperature of the reference forest station. Thus we collected the land surface temperature at the location of the TYW station (LST_{TYW}) observed by L5 / TM from 2000 to 2015 and then regressed LST_{TYW} and air temperature observed

at the TYW meteorological station (Figure 9). These results show that there is very good relationship between the forest surface temperature and air temperature at TYW station, thus we used the air temperature at the same time as the HR image observation to estimate the surface temperature at the TYW station. The air temperature of TYW at 12:10 p.m. on Oct 24, 2017 was 298.55 K and thus the forest surface temperature was 298.76 K. SUHIr and SUHIIc were calculated using this reference temperature. Generally, SUHIr was higher than SUHIIc. The mean SUHIr was 10.88 K with 3.90 K standard deviation, and mean SUHIIc was 8.60 K with 4.00 K standard deviation. Since the SUHIr is estimated using the nadir-view surface temperature, the exitance is dominated by roof and ground facets, which receive more solar irradiance at noon. Thus the SUHIr was higher than SUHIIc. This is consistent with the results from satellite data. Since the number of SUHIIc estimates from HR is very limited, the negative value does not appear in the HR estimates of SUHII-s. The HR data (Figure 5) did show that some facets' surface temperature is lower than the reference forest surface temperature. This may result in the urban cool island phenomenon.

4.2 | Impact of urban geometry on SUHIIs

We analysed the relationship between the building density, height, SVF and building height difference and SUHIIs.

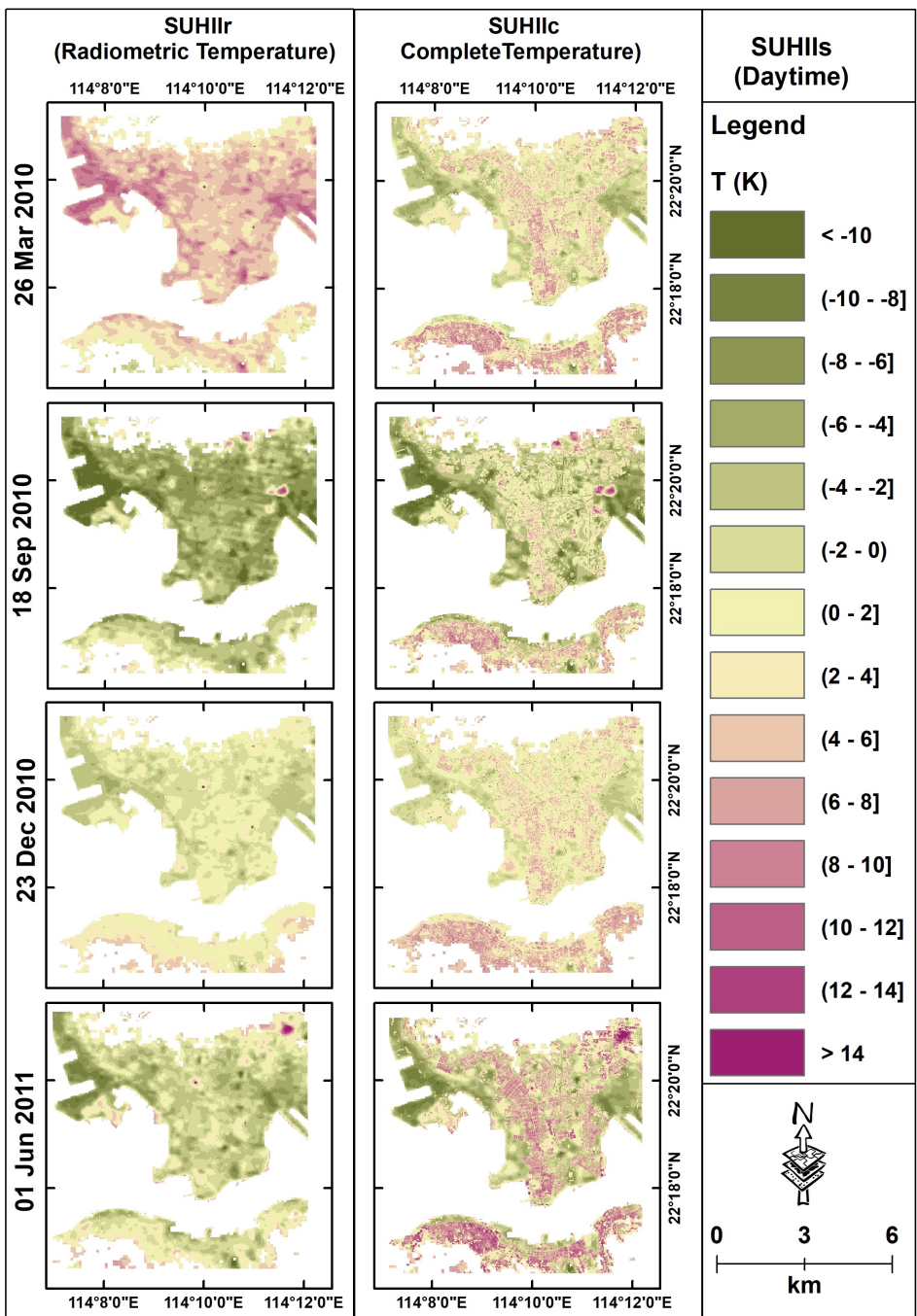


FIGURE 7 SUHII from Landsat data in the daytime

Both daytime SUHIIr and SUHIIc estimated using the Landsat TM LST retrievals are well correlated with these urban geometric parameters (Figure 10). Results showed that the geometric parameters have different impacts on SUHIIr and SUHIIc, that is, larger impacts on SUHIIc, while the building height and density have only slight impacts on SUHIIr. The slopes of the relationship between building height and SUHIIc are larger than that between building height and SUHIIr (Figure 10(a)), thus suggesting a higher sensitivity of SUHIIc to urban geometry. The slopes of SUHIIc vs. building density are also much larger than that between SUHIIr and building

density (Figure 10(b)). Table 3 shows the regressions between SUHIIc, SUHIIr and geometric parameters. The SUHIIc decreases with both building height and density, because of the decrease in irradiance on wall facets and, therefore, of wall temperature, while SUHIIr has limited sensitivity to building height and density, with building height having a larger impact on SUHIIr than building density. The latter is likely due to the increase of building height reducing the street temperature by shading, while the fractional roof cover does not change much. In this case, SUHIIr decreases slightly with increasing building height, while the impact of building density on SUHIIr is

FIGURE 8 SUHII from ASTER at nighttime

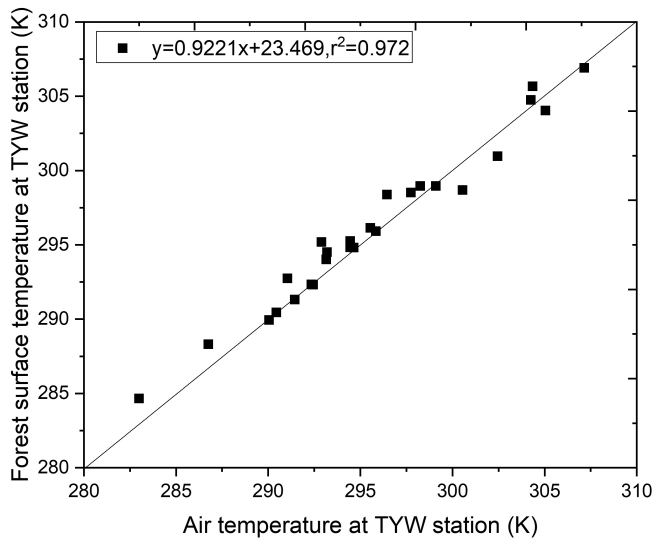
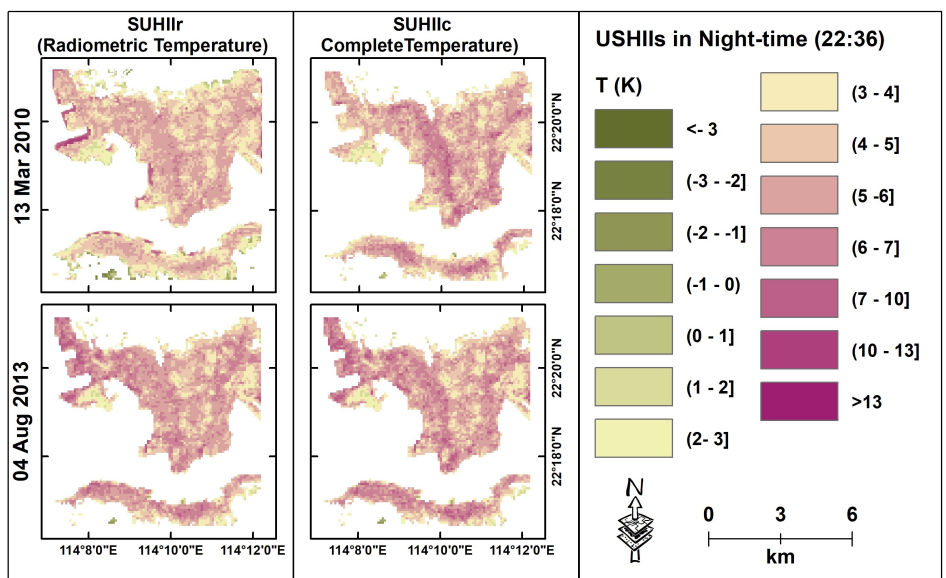


FIGURE 9 Relationship between air and forest surface temperature at TYW station

barely observable. In daytime, the change of SUHIIr with building density is limited, because it is the result of two contrasting effects. On the one hand, the street surface temperature decreases with increasing building density, on the other hand, the fractional abundance of roof facets increases with building density, which tends to increase SUHIIr because roofs are warmer than streets. Both SUHIIc and SUHIIr increase with SVF (Figure 10(c)). This is because a larger SVF increases irradiance onto urban facets, thus increasing both street and wall temperature. It should be noted that SUHIIc has a higher sensitivity to SVF than SUHIIr, as shown by the slopes of the relationships in Figure 10(c). Another relevant feature is that both SUHIIc and SUHIIr decrease with building

height variance (Figure 10(d)), i.e., with increasing shadows and aerodynamic roughness, with the latter increasing convective heat dissipation (Yang *et al.*, 2016a). Overall, the impact of SVF and building height variance on SUHIIc is larger than the impact of building height and density on SUHIIr. A complete picture of the sensitivity of SUHIIc and SUHIIr to urban geometric parameters is provided by the slopes of the linear regressions in Table 3. Overall, the sensitivity of SUHIIc to geometric parameters is higher than SUHIIr, as shown by the larger slopes of relationships applying to SUHIIc. These results indicate that the geometry of the built-up space has a larger impact on SUHIIc than on SUHIIr, that is, SUHIIc can better represent the difference in land surface process between urban and rural areas.

The impact of geometric parameters on SUHII in nighttime (Figure 11) is different than in daytime, since the dominant forcing during night time is longwave radiative and convective transfer. This mitigates the impact of urban geometry on SUHII in nighttime, although the geometry impacts on SUHIIc are still higher than that on SUHIIr. Higher building height captures more longwave radiation and reduces heat dissipation, thus increasing both SUHIIc and SUHIIr. More specifically, higher buildings lead to higher street and wall surface temperatures, which implies higher SUHIIr and SUHIIc. Like daytime, in nighttime SUHIIc is more sensitive to building height (i.e., steeper slope) than SUHIIr (Figure 11(a)). In nighttime both SUHIIc and SUHIIr increase with building density (Figure 11(b)), since higher building density captures better the radiative energy and reduces convective heat transfer. This increases the street and wall surface temperature, thus SUHIIc and SUHIIr. Again, SUHIIc is

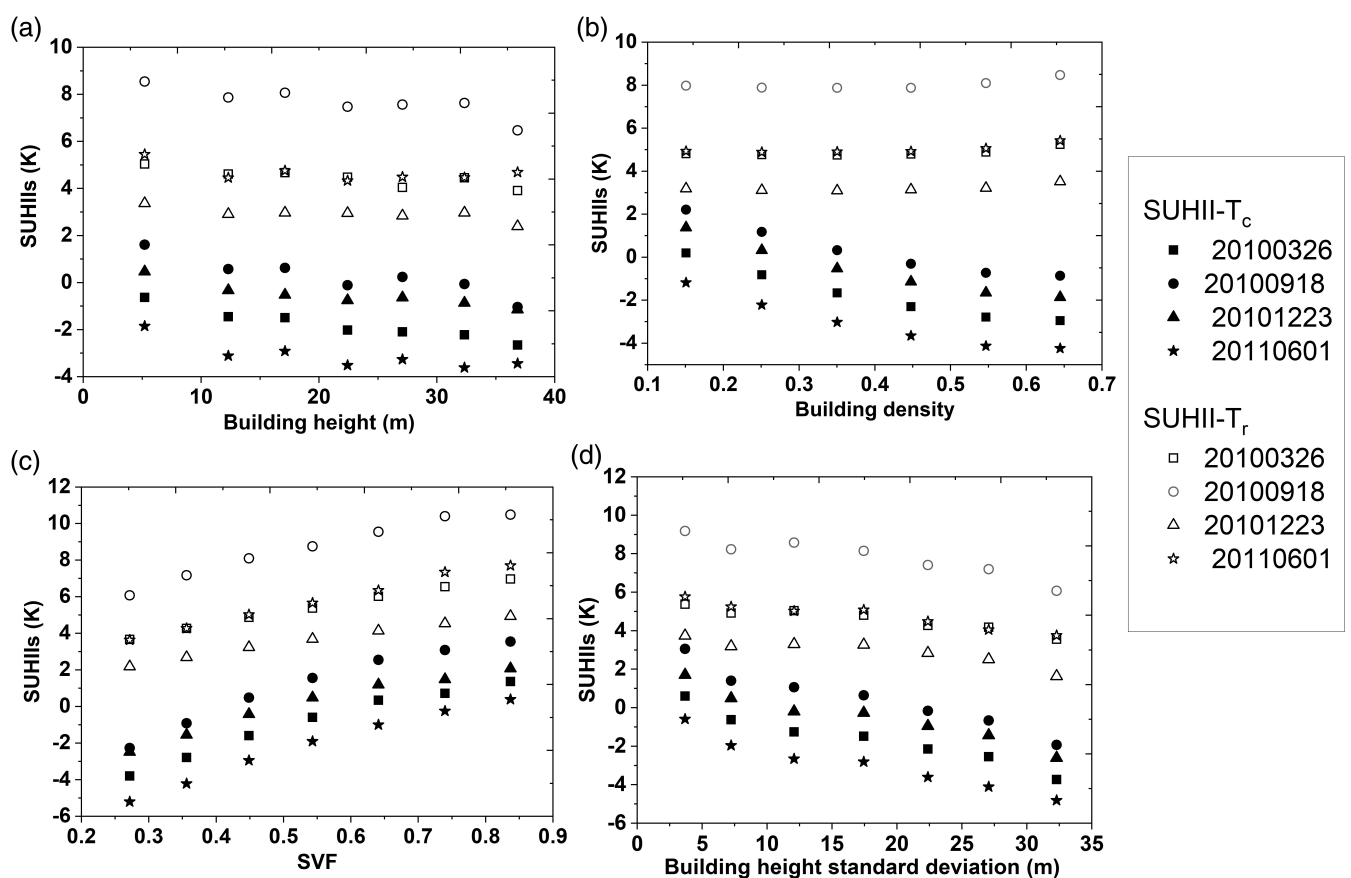


FIGURE 10 Relationships between SUHIIIs from daytime Landsat data and geometric parameters: (a), building height; (b), building density; (c), SVF; (d), building height standard deviation

more sensitive to density (i.e., steeper slope) than SUHIIr (Table 3). Higher SVF increases heat dissipation by convection and longwave radiation by emission to the atmosphere, thus reducing both wall and street surface temperature, that is, both SUHIIc and SUHIIr (Figure 11(c)). The sensitivity of SUHIIIs (Figure 11(c)) was lower than the sensitivity of UHI_{max} to SVF (See Figure 7.13 on Page 216 presented by Oke *et al.* (2017)). This may be because roof surface temperature is insensitive to SVF and the fractional abundance of roof facets increases with decreasing SVF. The nighttime impact of building height variance on SUHIIc and SUHIIr is complex. At lower building height variance SUHIIc and SUHIIr increase slightly, then both SUHII and SUHIIr level off (Figure 11(d)). During nighttime the building height variance mainly affects convective heat transfer through aerodynamic roughness, which has a smoother impact than directly through irradiance in daytime. In this sense, increasing the building height difference is good for heat mitigation at daytime and nighttime when the building density cannot change.

The dependence of is the relationships between SUHIIIs on and geometric parameters has also been

evaluated using the HR data (Figure 12 and Table 4). Both SUHIIr and SUHIIc increase with SVF and the slope of the relationship between SUHIIc and SVF is larger than that between SUHIIr and SVF. SUHIIr slightly increases with building density while SUHIIc decreases with building density. Both SUHIIr and SUHIIc decrease with building height and building height standard deviation or difference. The slopes of the relationship between SUHIIc and building height/building height standard deviation are larger than for SUHIIr. The results based on HR data are consistent with the ones obtained with Landsat TM data and the estimated T_c , although the number of data is limited. This means the T_c estimated by an empirical relationship based on Yang *et al.* (2020a) captures the geometric effects correctly.

4.3 | Difference between UHII and SUHIIIs

To assess whether SUHIIIs and UHI are related, we compared the SUHIIc and SUHIIr with UHII, which is based

TABLE 3 Linear regression equations relating SUHIIc and SUHIIr to urban geometric parameters

Date	Regression and correlation coefficients		Building height		SVF		Building height variance	
	SUHIIc	SUHIIr	SUHIIc	SUHIIr	SUHIIc	SUHIIr	SUHIIc	SUHIIr
Mar 26, 2010	$y = -0.453x + 0.854$, $r^2 = 0.950$	$y = 0.729x + 4.583$, $r^2 = 0.531$	$y = -0.057x + 0.543$, $r^2 = 0.941$	$y = -0.030x + 5.120$, $r^2 = 0.77$	$y = 9.160x - 5.925$, $r^2 = 0.971$	$y = 5.871x + 2.171$, $r^2 = 0.996$	$y = -0.13x + 0.662$, $r^2 = 0.951$	$y = -0.057x + 5.580$, $r^2 = 0.9174$
Sept 18, 2010	$y = -0.278x + 2.806$, $r^2 = 0.938$	$y = 0.888x + 7.677$, $r^2 = 0.497$	$y = -0.067x + 1.729$, $r^2 = 0.846$	$y = -0.049x + 8.750$, $r^2 = 0.76$	$y = 10.311x - 4.503$, $r^2 = 0.957$	$y = 7.931x + 4.3$, $r^2 = 0.97$	$y = -0.149x + 3.078$, $r^2 = 0.944$	$y = -0.092x + 9.441$, $r^2 = 0.892$
Dec 23, 2010	$y = -6.572x + 2.040$, $r^2 = 0.934$	$y = 0.577x + 2.987$, $r^2 = 0.462$	$y = -0.042x + 0.387$, $r^2 = 0.857$	$y = -0.020x + 3.358$, $r^2 = 0.636$	$y = 8.015x - 4.2804$, $r^2 = 0.960$	$y = 4.834x + 0.978$, $r^2 = 0.993$	$y = -0.128x + 1.771$, $r^2 = 0.943$	$y = -0.060x + 3.397$, $r^2 = 0.832$
Jun 1, 2011	$y = -6.273x + 0.575$, $r^2 = 0.9417$	$y = 0.873x + 4.673$, $r^2 = 0.596$	$y = -0.044x + 2.140$, $r^2 = 0.671$	$y = -0.019x + 5.080$, $r^2 = 0.3179$	$y = 10.016x - 7.650$, $r^2 = 0.9844$	$y = 7.410x + 1.648$, $r^2 = 0.995$	$y = -0.131x + 0.654$, $r^2 = 0.947$	$y = -0.066x + 5.916$, $r^2 = 0.945$
Mar 13, 2013	$y = 3.923x + 4.306$, $r^2 = 0.959$	$y = 0.607x + 4.670$, $r^2 = 0.581$	$y = 0.014x + 4.017$, $r^2 = 0.3406$	$y = -0.0055x + 3.3804$, $r^2 = 0.502$	$y = -2.855x + 6.855$, $r^2 = 0.994$	$y = -1.719x + 5.644$, $r^2 = 0.904$	$y = 0.0275x + 4.938$, $r^2 = 0.459$	$y = 0.013x + 4.455$, $r^2 = 0.161$
Aug 4, 2013	$y = 4.438x + 4.103$, $r^2 = 0.995$	$y = 1.163x + 4.956$, $r^2 = 0.933$	$y = 0.026x + 3.848$, $r^2 = 0.6757$	$y = 0.0184x + 3.7021$, $r^2 = 0.407$	$y = -1.226x + 6.06$, $r^2 = 0.699$	$y = 0.0358x + 5.290$, $r^2 = 0.010$	$y = 0.018x + 5.180$, $r^2 = 0.620$	$y = 0.0036x + 5.2207$, $r^2 = 0.063$

on air temperature (Figure 13). Both SUHIIc and SUHIIr are positively correlated with UHI, as expected, although these correlations are relatively weak. SUHIIc values are closer to UHII's than SUHIIr's and the correlation coefficient between SUHIIc and UHII is higher than that between SUHIIr and UHII. This is because the air temperature within the urban canopy is more affected by ground and surrounding wall facets, while roof facets have very little impact on the air temperature near the ground within the urban canopy, especially for the high building (Ng *et al.*, 2012). In this sense, T_c should be used for urban climate research, instead of T_r .

The solar zenith angle depends on Day of Year (DoY). Different solar zenith angle implies changes in irradiance and the duration of both illumination and shadowing, leading to different values, spatial distribution and evolution of surface temperature, which are likely to result in a difference between radiometric and complete surface temperature. The solar zenith angle has been considered in the estimation of T_c from radiometric surface temperature, thus was not considered explicitly in the comparison between SUHII and UHII.

5 | DISCUSSION

The difference between T_c and T_r has been addressed in several studies (Voogt and Oke, 1997; Adderley *et al.*, 2015; Allen *et al.*, 2018; Jiang *et al.*, 2018), which documented the large difference between complete and radiometric surface temperature. This study compared the evaluation of SUHII using either nadir-viewed radiometric or complete surface temperature based on satellite thermal images and high-resolution airborne images. As T_c and T_r are different in nature, SUHIIr and SUHIIc have different magnitude and spatial patterns. Additionally, urban geometry has different effects on SUHIIr and SUHIIc, and even some geometric parameters have contrary effects on SUHIIr and SUHIIc, because radiometric and complete surface temperature represent different facet information. This further revealed how the urban geometry determines the urban surface temperature for different components.

Several studies compared the UHI based on air temperature observed at meteorological stations and the radiometric surface temperature observed from satellite thermal data (Sun *et al.*, 2015; Zhou *et al.*, 2019), while the difference between the radiometric surface temperatures observed by nadir-viewing radiometers and complete surface temperature to estimate SUHII have not been evaluated. Thus, this study also compared SUHIIc and SUHIIr with UHII in Hong Kong.

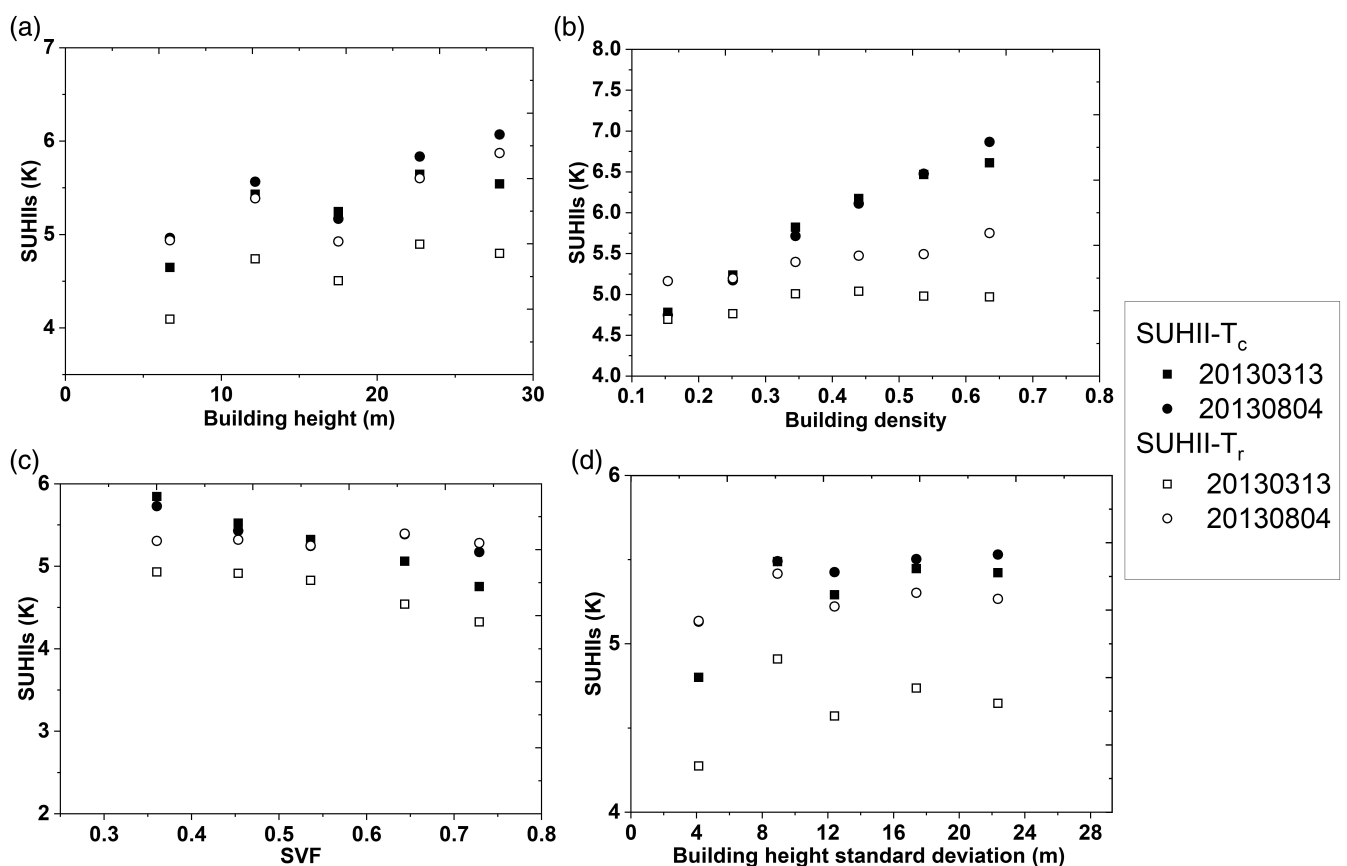


FIGURE 11 Relationships between SUHII from nighttime ASTER data and geometric parameters: (a), building height; (b), building density; (c), SVF; (d), building height standard deviation

The implications of our study relate to three main aspects: a) the use of observations of urban air and surface temperature in relation with the footprint of the observations; b) the interpretation of UHI, SUHIIr and SUHIIc in relation with the characteristics of the built-up space; and c) expected impact of changes in urban geometry on SUHII.

For a), clearly, air and surface temperature are different geophysical variables in many ways, particularly their footprints (Oke *et al.*, 2017). Measuring air temperature at a point captures a signal originating in the source area of the sampled air flow. Footprint of air temperature depends on air flow in the boundary layer and increases with the time of integration of the measurement. On the other hand, the footprint of a radiometric measurement of surface temperature is precisely defined by the Field of View of the instrument and varies between different sensors. In general, it is different from the footprint of an air temperature measurement, which relates to the source area, that is, the area of the surface upwind of an air temperature probe that influences the measurements made at that point. The source area size depends on the height of the air temperature probe, wind direction, stability and surface roughness. An accurate estimates of the size and shape of the footprint of air temperature measurements

in urban areas is very complex (Hellsten *et al.*, 2015). Advanced modelling is required to capture the interaction of boundary layer conditions, turbulent flow and the geometry of the urban canopy. The numerical experiments of Hellsten *et al.* (2015) suggest that the signal captured by an air temperature measurement at 10 m height is likely to originate from a source area up to a factor 10² larger in the wind direction and up a factor 10 in the crosswind direction. Accordingly, the difference in footprint size and shape should be taken into account when applying observations of surface and air temperature to local analyses of the impact of urban geometry. This implies that the air and surface temperatures convey information on the impact of the built-up space on the surface energy balance at rather different spatial scales. If the impact of the built-up environment on weather and climate is the research objective, air temperature can meet efficiently such requirements, while a map of surface temperature at high spatial resolution would require spatial averaging. Contrariwise, if a better understanding is being sought of the impact of urban geometry and materials on the thermal conditions within urban canyons at micro-scale, measurements of the surface temperature of all the relevant facets would be a better solution.

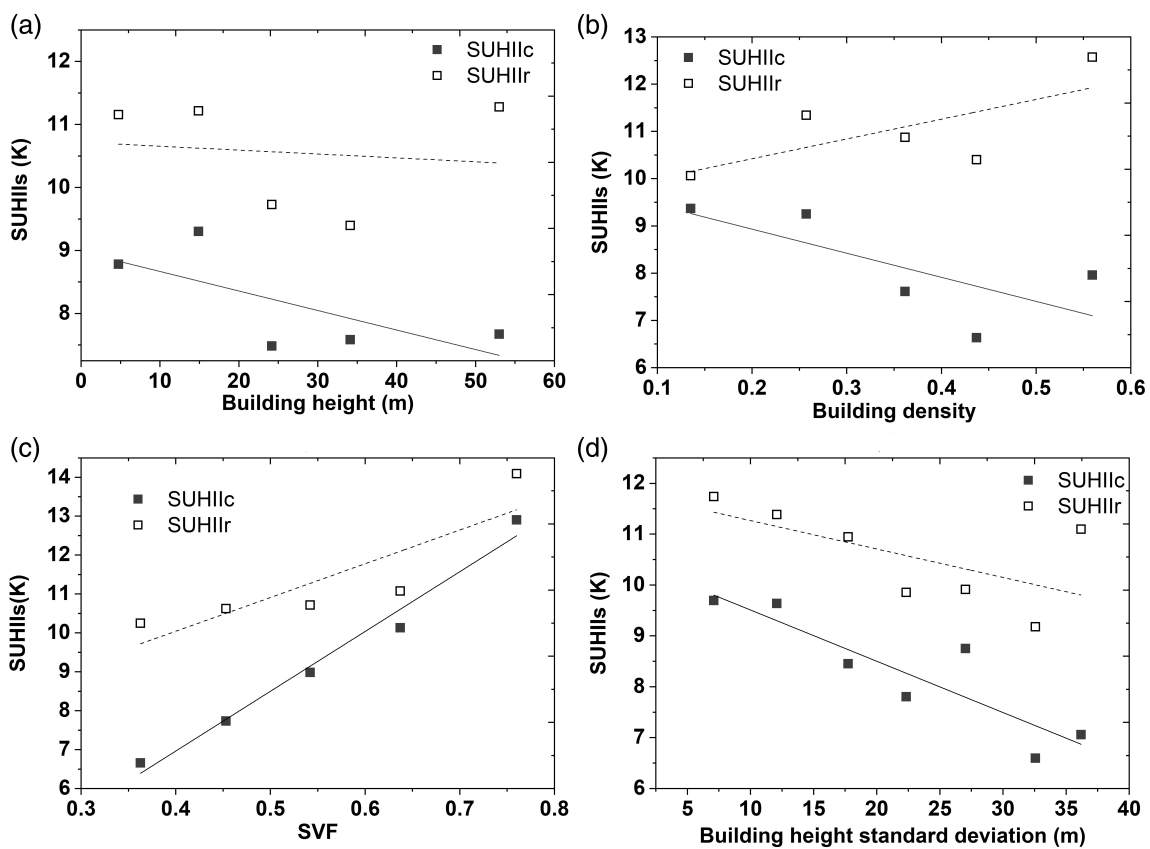


FIGURE 12 Relationships between SUHII-s from daytime HR data and geometric parameters: (a), building height; (b), building density; (c), SVF; (d), building height standard deviation

For b), the difference between SUHIIc and SUHIIr in very dense built-up areas is larger than in flat impervious areas, because this condition makes the difference between complete and radiometric surface temperature larger than the condition of impervious flat areas. This is very obvious in Hong Kong because it is a highly compact city. Considering the buildings in Hong Kong are very tall and narrow, the total wall area may even be higher than the urban horizontal surface area. Wall surface temperatures are important components of the urban climate but are under-sampled by satellite and airborne remote sensing (Hilland and Voogt, 2020). SUHIIr based on radiometric surface temperature may cause a large bias in assessments of SUHI in Hong Kong.

For c), both UHI and SUHI are useful metrics to assess impacts of the design and management of urban space on urban climate and residents, including increasing the energy consumption to cool indoor spaces and heat stress on human residents in summer (Oke *et al.*, 2017). The sensitivity of SUHIIr and SUHIIc to urban geometry, documented by our study, provides useful insights as regards: expected changes in urban climate in response to the evolution of urban space, specifically to changes in the urban geometric parameters we have

considered; indications about adaptations in urban design that would contribute to mitigating the impacts of climate variability, specifically which changes in urban geometric parameters would be needed to achieve a given (target) change in SUHII-s;

Our results are preliminary and further evaluation by numerical experiments and in-situ measurements is needed, but they document the sensitivity of SUHII to urban geometry.

In this context, we should take into account that higher urban surface temperature may save energy for winter heating and improve the thermal comfort. SUHII-s are not necessarily an indicator applicable for this purpose due to the variability of rural surface temperature and the impact of the rural reference temperature on estimated SUHII-s (Martilli *et al.*, 2020a; Martilli *et al.*, 2020b). On another count, considering that Hong Kong is a very densely built city with a long summer season, our results suggest that the aerodynamic roughness of the urban canopy should be increased to improve heat dissipation. The building density, height, height difference and SVF have different impacts on SUHIIr and SUHIIc. Compared with other geometric parameters, building height variance has most significant effects on

TABLE 4 Linear regression equations relating SUHIIc and SUHIIr to urban geometric parameters of Oct 24, 2017

Regression and correlation coefficients			
Date	Building density	Building height	SVF
SUHIIr	$y = 4.1839x + 9.5886$ $R^2 = 0.486$	$y = -0.0062x + 10.718$ $R^2 = 0.015$	$y = 8.6714x + 6.5776$ $R^2 = 0.742$
SUHIIc	$y = -5.0957x + 9.9511$ $R^2 = 0.520$	$y = -0.031x + 8.9774$ $R^2 = 0.485$	$y = 15.363x + 0.8214$ $R^2 = 0.9789$

SUHIIr and SUHIIc in daytime. For night time, the building height difference or variance does not lead to a significant increase in SUHIIr and SUHIIc. This means that the building height variance is an effective urban property to improve urban heat dissipation in daytime. This can be achieved by increasing the building height variance if other geometric parameters cannot be changed in Hong Kong.

The main contribution of this study is the evaluation of monitoring the SUHI using T_c instead of T_r . To this end, we have used estimates of T_c with the error of estimate documented in our previous study (Yang *et al.*, 2020a). The error of estimate may have a three-fold impact on our analyses: (1) the impact of systematic error in the estimated T_c on the assessed SUHIIc and, therefore, on the comparative analysis of SUHIIc and SUHIIr; (2) the significance of SUHIIc estimates, given the random error on T_c ; (3) the interpretation of the estimated RMSE, given the different nature of T_c retrievals based on Yang *et al.* (2020a) and the ones obtained directly from the 0.2 m x 0.2 m resolution TIR data.

As regards (1), we have used the offset (b) in the regression $T_c = aT_r + b$ (see Yang *et al.*, 2020a for further details) as an estimate of bias on T_c , although this assumption is only applicable when $a \approx 1$. We obtained $b = 4.60$ K (daytime) and $b = 2.60$ K (nighttime). On the other hand, the results presented in this study indicate that overall SUHIIc < SUHIIr, thus suggesting that the bias on T_c had a limited impact on our conclusions on SUHIIc vs. SUHIIr. As regards (2), we have compared first the RMSE values in Yang *et al.* (2020a), i.e., 1.5 K (daytime) and 0.69 K (nighttime) with the distributions of SUHIIc either as estimated according to Yang *et al.* (2020a), see Figure 14, or retrieved from the 0.2 m x 0.2 m spatial resolution data (Figure 15). In all cases, the RMSE is about 10% of the range of estimated SUHIIc.

Thus, the impact of such error on the estimated SUHIIc is rather limited. Another aspect related to the bias on the SUHIIc estimates is that a different choice of the rural reference may lead to a large bias on the values in either SUHII (Yao *et al.*, 2019; Li *et al.*, 2020). This question was not investigated in this study, however. The geometry of vegetation canopies is inherently 3D, thus measurements of the surface temperature pose similar challenges as with urban surface temperature. We did not address such challenges, but we plan to extend our studies of SUHI to include both urban and rural vegetation.

As regards (3), it should be noted that the estimated T_c is retrieved from radiances measured with a footprint roughly 100 m in diameter, further downscaled to 30 m x 30 m in the L5/TM data products. This means that the TM instrument captures a radiance averaged over

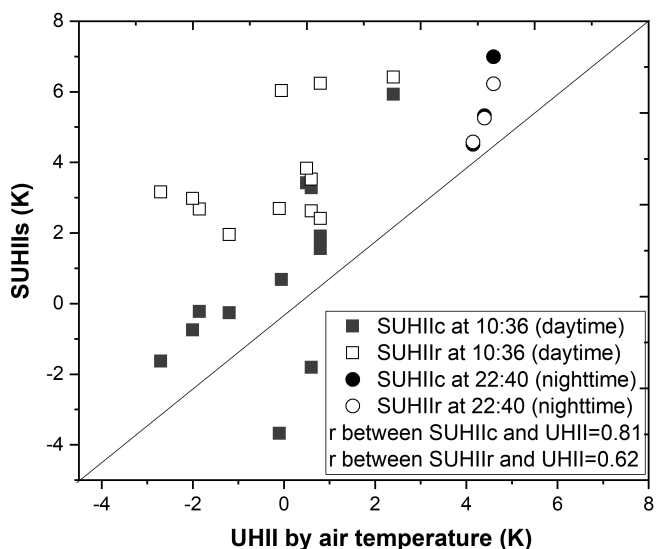


FIGURE 13 Comparison between SUHII and UHI

different facets within a footprint, thus filtering out inherent differences in facet surface temperature. On the contrary, the high resolution T_c is retrieved from exitance measurements of single facets, then averaging by facet type for each 100 m \times 100 m grid. This preserves the differences between facets and to some extent their spatial organization. This procedure is similar to the one applied by Yang *et al.* (2020a) to estimate T_c . This implies that

the RMSE given in Yang *et al.* (2020a) applies better to the high resolution than to the satellite retrievals of T_c . In conclusion, the RMSE should be compared with the distribution of T_c and SUHIIc determined with the high resolution TIR data to conclude that the impact of the error of estimate associated with the method of Yang *et al.* (2020a) is limited.

This study also has several limitations. For HR data, we directly used the observed facets to estimate T_c . Although we tried best to obtain all facets which were captured by the HR data of different flight-lines, there are still some facets which cannot be seen and we could not completely correct for image distortion. Both of these factors may result in a bias on estimated T_c . Despite these limitations, T_c estimated from HR data can still convey more information than the nadir-view radiometric temperature. For satellite data, the main limitation is the estimation of complete surface temperature used in this study, which does not include the effects of vegetation and variable building shape and spatial arrangement because TUF-3D only simulates the surface temperature of uniform spatial arrangements in the built-up space without vegetation. The spatial arrangement is the pattern in position, orientation and spacing of buildings. These patterns change the shadow and thermal distribution, which is likely to have an impact on the estimated difference between radiometric and complete surface temperature. In each numerical experiment with TUF –

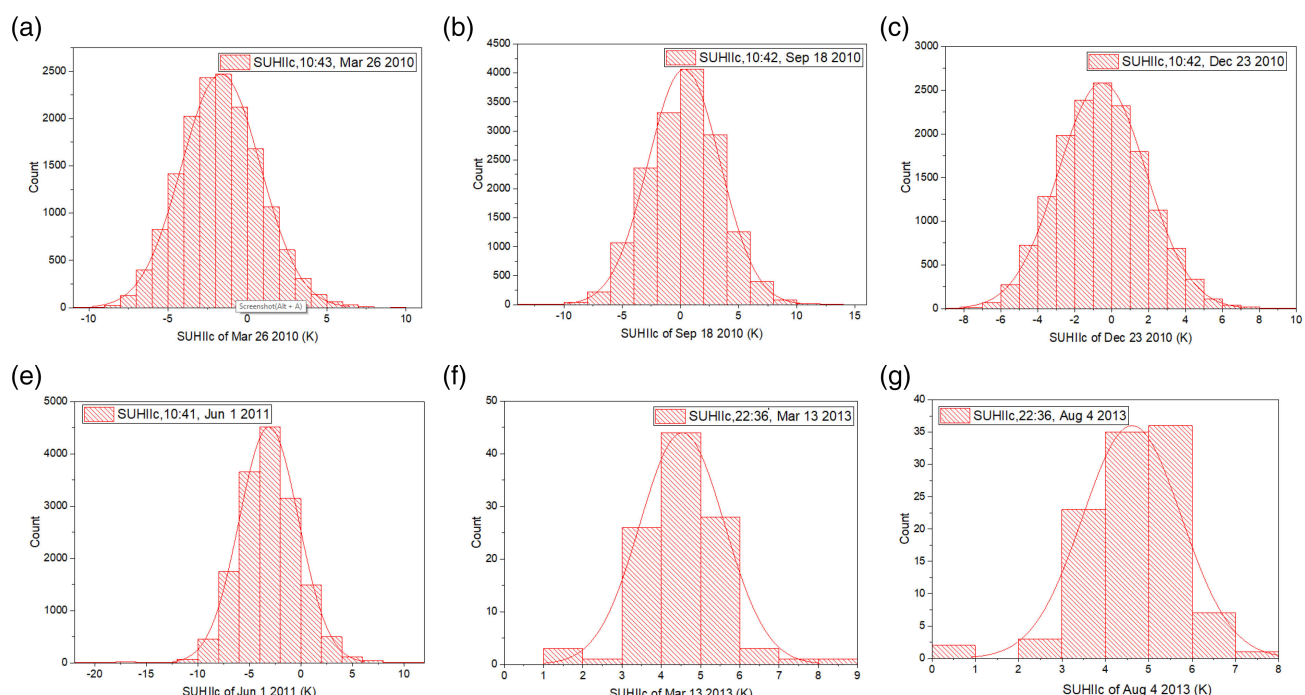


FIGURE 14 Frequency distribution of SUHIIc from satellite data: a, b, c, and d are daytime images acquired by L5 / TM; e and f are nighttime images acquired by ASTER

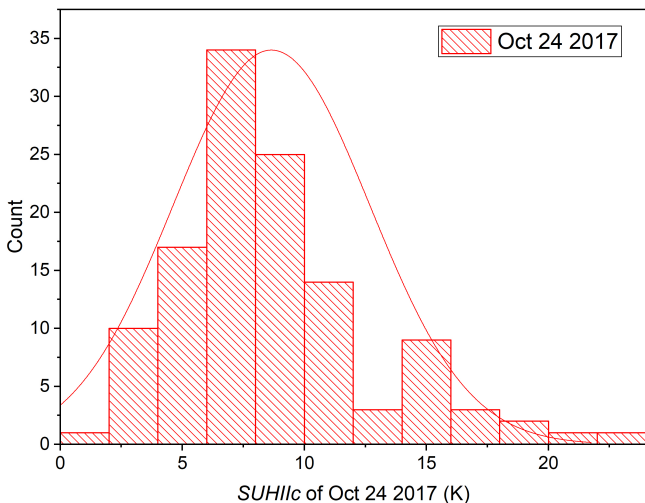


FIGURE 15 Frequency distribution of SUHIIc retrieved from the 0.2 m x 0.2 m spatial resolution data

3D the spatial arrangement of buildings must be uniform over the domain, but we performed multiple experiments by changing the arrangement of buildings.

This method estimates T_c from T_r using information on urban geometry because T_c cannot directly be observed by a nadir-looking, space-borne imaging radiometer. The estimated T_c was in good agreement with both experimental and model reference values. In our view, this shows that our T_c estimates capture the effect of urban geometry on SUHI better than T_r . The land cover and vegetation effects are not discussed in this study because the impact of these factors on SUHIIr and UHII has been studied thoroughly in previous studies.

Another limitation is the comparison of SUHIIr and SUHIIc with UHII based on station-measured air temperature. The difference between SUHI and UHI has been studied using the urban radiometric surface temperature and the air temperature observed within the urban canopy (Sun *et al.*, 2015; Hu *et al.*, 2019), which documented that the land cover and urban climate affect the difference between SUHIIr and UHII. Zhou *et al.* (2019) analysed the rural–urban temperature variability in Israel based on different temperatures which are measured air temperature near surface, satellite-observed temperature and simulated canopy air temperature and results showed that different temperatures might lead to contrasting results, with a radiometric surface temperature being dominated by the emittance of horizontal facets. Although SUHIIc showed a better agreement with UHII than SUHIIr, the UHII is based on very limited measured data. We hope more air temperature measurements collected by mobile platforms can be obtained to study the geometry effects on UHII.

6 | CONCLUSIONS

This study mapped the SUHII using both radiometric and complete surface temperature to document and understand the difference between SUHIIc and SUHIIr. The urban cool island effect appeared at places with denser buildings when evaluating SUHIIc, while SUHIIr did not capture this effect. SUHIIc is more sensitive to urban geometric parameters than SUHIIr, since geometry affects all facet temperatures, while T_r mainly captures roof and street temperature. The geometric parameters have different effects on SUHIIr and SUHIIc at daytime and nighttime and even contrary effects on SUHIIr and SUHIIc at daytime. The building height variance and SVF become an important determinant of SUHII. Building height variance has the most significant effects on reducing SUHIIr and SUHIIc in daytime. In night time, the building height variance does not lead to a significant increase in either SUHIIr or SUHIIc. Thus building height variance might be increased to mitigate urban heat stress if other parameters cannot be changed. Likewise SUHIIc, UHI revealed the urban cool island effect in daytime. The comparison between SUHIIc and UHII showed that the SUHIIc is much closer to UHII than SUHIIr. SUHIIc should be used for SUHI study because it better captures urban microclimate.

ACKNOWLEDGEMENT

This work was supported by Grants by National Natural Science Foundation of China (41901283, 61976234) and the Team Project of Guangdong Provincial Natural Science Foundation (2018B030312004). The authors thank the Hong Kong Planning Department, Hong Kong Lands Department, the Hong Kong Civil Engineering and Development Department, the Hong Kong Observatory and the Hong Kong Government Flying Service for the planning, building GIS, weather and climate, and airborne Lidar data, and NASA LP DAAC for the Landsat and ASTER satellite imagery. Massimo Menenti acknowledges the support of grant P10-TIC-6114 by the Junta de Andalucía and the MOST High Level Foreign Expert program (Grant nr. G2019016 1018). Man Sing Wong thanks the funding support from a grant by the General Research Fund (Grant no. 15602619) from the Hong Kong Research Grants Council. We acknowledge the two anonymous reviewers' and editor's very useful comments to help us to improve this manuscript.

CONFLICT OF INTEREST

The authors declare no conflict of interest.

ORCID

- Jinxin Yang  <https://orcid.org/0000-0002-8383-9922>
 Man Sing Wong  <https://orcid.org/0000-0002-6439-6775>
 Sawaid Abbas  <https://orcid.org/0000-0003-3417-217X>

REFERENCES

- Adderley, C., Christen, A. and Voogt, J.A. (2015) The effect of radiometer placement and view on inferred directional and hemispheric radiometric temperatures of an urban canopy. *Atmospheric Measurement Techniques*, 8(7), 2699–2714.
- Allen, M., Voogt, J. and Christen, A. (2018) Time-continuous hemispherical urban surface temperatures. *Remote Sensing*, 10(1), 3.
- Carnahan, W.H. and Larson, R.C. (1990) An analysis of an urban heat sink. *Remote Sensing of Environment*, 33(1), 65–71.
- Chen, L., Ng, E., An, X., Ren, C., Lee, M., Wang, U. and He, Z. (2012) Sky view factor analysis of street canyons and its implications for daytime intra-urban air temperature differentials in high-rise, high-density urban areas of Hong Kong: a GIS-based simulation approach. *International Journal of Climatology*, 32 (1), 121–136.
- Chen, X.-L., Zhao, H.-M., Li, P.-X. and Yin, Z.-Y. (2006) Remote sensing image-based analysis of the relationship between urban heat Island and land use/cover changes. *Remote Sensing of Environment*, 104(2), 133–146.
- Crawford, B., Krayenhoff, E.S. and Cordy, P. (2018) The urban energy balance of a lightweight low-rise neighborhood in Andacollo, Chile. *Theoretical and Applied Climatology*, 131, 55–68. <https://doi.org/10.1007/s00704-016-1922-7>.
- Hellsten, S.M., Luukkonen, G., Steinfeld, F., Kanani-Sühring, T., Markkanen, L., Järvi, J., Lento, T. and Vesala, S.R. (2015) Footprint evaluation for flux and concentration measurements for an urban-like canopy with coupled Lagrangian stochastic and large-Eddy simulation models. *Boundary-Layer Meteorol.*, 157, 191–217.
- Hilland, R.V.J. and Voogt, J.A. (2020) The effect of sub-facet scale surface structure on wall brightness temperatures at multiple scales. *Theoretical and Applied Climatology*, 140, 767–785.
- Hu, L. and Brunsell, N.A. (2013) The impact of temporal aggregation of land surface temperature data for surface urban heat Island (SUHI) monitoring. *Remote Sensing of Environment*, 134, 162–174.
- Hu, Y., Hou, M., Jia, G., Zhao, C., Zhen, X. and Xu, Y. (2019) Comparison of surface and canopy urban heat islands within megacities of eastern China. *ISPRS Journal of Photogrammetry and Remote Sensing*, 156, 160–168.
- Huang, F., Zhan, W., Voogt, J., Hu, L., Wang, Z., Quan, J., Ju, W. and Guo, Z. (2016) Temporal upscaling of surface urban heat Island by incorporating an annual temperature cycle model: a tale of two cities. *Remote Sensing of Environment*, 186, 1–12.
- Huang, X. and Wang, Y. (2019) Investigating the effects of 3D urban morphology on the surface urban heat Island effect in urban functional zones by using high-resolution remote sensing data: a case study of Wuhan, Central China. *ISPRS Journal of Photogrammetry and Remote Sensing*, 152, 119–131.
- Jiang, L., Zhan, W., Voogt, J., Zhao, L., Gao, L., Huang, F., Cai, Z. and Ju, W. (2018) Remote estimation of complete urban surface temperature using only directional radiometric temperatures. *Building and Environment*, 135, 224–236.
- Krayenhoff, E.S. and Voogt, J. (2007) A microscale three-dimensional urban energy balance model for studying surface temperatures. *Boundary-Layer Meteorology*, 123(3), 433–461.
- Krayenhoff, E.S., Christen, A., Martilli, A., & Oke, T.R. (2014). A Multi-layer Radiation Model for Urban Neighbourhoods with Trees. *Boundary-Layer Meteorology*, 151, 139–178.
- Krayenhoff, E.S. and Voogt, J.A. (2016) Daytime thermal anisotropy of urban Neighbourhoods: morphological causation. *Remote Sensing*, 8(2), 108.
- Kuang, W., Dou, Y., Zhang, C., Chi, W., Liu, A., Liu, Y., Zhang, R. and Liu, J. (2015) Quantifying the heat flux regulation of metropolitan land use/land cover components by coupling remote sensing modeling with in situ measurement. *Journal of Geophysical Research: Atmospheres*, 120(1), 113–130.
- Lagouarde, J.-P., Hénon, A., Irvine, M., Voogt, J., Pigeon, G., Moreau, P., Masson, V. and Mestayer, P. (2012) Experimental characterization and modelling of the nighttime directional anisotropy of thermal infrared measurements over an urban area: case study of Toulouse (France). *Remote Sensing of Environment*, 117, 19–33.
- Lagouarde, J.P., Hénon, A., Kurz, B., Moreau, P., Irvine, M., Voogt, J. and Mestayer, P. (2010) Modelling daytime thermal infrared directional anisotropy over Toulouse city Centre. *Remote Sensing of Environment*, 114(1), 87–105.
- Li, J., Wang, F., Fu, Y., Guo, B., Zhao, Y. and Yu, H., 2020. A novel SUHI referenced estimation method in multi-centers urban agglomeration with DMSP/OLS nighttime light data. *IEEE Journal of Selected Topics in Applied Earth Observations and Remote Sensing*, 13, 1416–1425. <https://doi.org/10.1109/JSTARS.2020.2981285>.
- Li, N. and Li, X. (2020) The impact of building thermal anisotropy on surface urban Heat Island intensity estimation: An observational case study in Beijing. *IEEE Geoscience and Remote Sensing Letters*, 1–5. <https://doi.org/10.1109/LGRS.2019.2962383>.
- Li, X., Li, W., Middel, A., Harlan, S.L., Brazel, A.J. and Turner, B.L. (2016) Remote sensing of the surface urban heat Island and land architecture in Phoenix, Arizona: combined effects of land composition and configuration and cadastral-demographic-economic factors. *Remote Sensing of Environment*, 174, 233–243.
- Martilli, A., Krayenhoff, E.S. and Nazarian, N. (2020a) Is the urban Heat Island intensity relevant for heat mitigation studies? *Urban Climate*, 31, 100541.
- Martilli, A., Roth, M., Chow, W., Demuzere, M., Lipson, M., Krayenhoff, E., Sailor, D., Nazarian, N., Voogt, J., Wouters, H., Middel, A., Stewart, I., Bechtel, B., Christen, A. and Hart, M., 2020b. *Summer Average Urban-Rural Surface Temperature Differences Do Not Indicate the Need for Urban Heat Reduction*. Bloomington, IL: OSF. <https://doi.org/10.31219/osf.io/8gnbf>.
- Ng, E., Chen, L., Wang, Y. and Yuan, C. (2012) A study on the cooling effects of greening in a high-density city: An experience from Hong Kong. *Building and Environment*, 47, 256–271.
- Oke, T., Cleugh, H., Grimmond, C., Schmid, H. and Roth, M. (1989) Evaluation of spatially-averaged fluxes of heat, mass and momentum in the urban boundary layer. *Weather and Climate*, 9, 14–21.
- Oke, T.R. (1981) Canyon geometry and the nocturnal urban heat Island: comparison of scale model and field observations. *Journal of Climatology*, 1(3), 237–254.

- Oke, T.R. (1982) The energetic basis of the urban heat Island. *Quarterly Journal of the Royal Meteorological Society*, 108(455), 1–24.
- Oke, T.R., Mills, G., Christen, A. and Voogt, J.A., 2017. *Urban Climates*. 1 Cambridge, England: Cambridge University Press. <https://doi.org/10.1017/9781139016476>.
- Oke, T.R., Spronken-Smith, R.A., Jáuregui, E. and Grimmond, C.S. B. (1999) The energy balance of Central Mexico City during the dry season. *Atmospheric Environment*, 33(24–25), 3919–3930.
- Peng, S., Piao, S., Ciais, P., Friedlingstein, P., Ottle, C., Bréon, F.-M., Nan, H., Zhou, L. and Myneni, R.B. (2012) Surface urban Heat Island across 419 global big cities. *Environmental Science & Technology*, 46(2), 696–703.
- Roth, M., Oke, T.R. and Emery, W.J. (1989) Satellite-derived urban heat islands from three coastal cities and the utilization of such data in urban climatology. *International Journal of Remote Sensing*, 10(11), 1699–1720.
- Shahmohamadi, P., Che-Ani, A., Ramly, A., Maulud, K. and Mohd-Nor, M. (2010) Reducing urban heat Island effects: a systematic review to achieve energy consumption balance. *International Journal of Physical Sciences*, 5(6), 626–636.
- Siu, L.W. & Hart, M.A. (2013). Quantifying urban heat island intensity in Hong Kong SAR, China. *Environmental Monitoring and Assessment*, 185, 4383–4398.
- Sobrino, J.A., Jiménez-Muñoz, J.C., Balick, L., Gillespie, A.R., Sabol, D.A. & Gustafson, W.T. (2007). Accuracy of ASTER Level-2 thermal-infrared Standard Products of an agricultural area in Spain. *Remote Sensing of Environment*, 106, 146–153.
- Stewart, I.D. (2011) A systematic review and scientific critique of methodology in modern urban heat Island literature. *International Journal of Climatology*, 31(2), 200–217.
- Sun, H., Chen, Y. and Zhan, W. (2015) Comparing surface- and canopy-layer urban heat islands over Beijing using MODIS data. *International Journal of Remote Sensing*, 36(21), 5448–5465.
- Voogt, J., 2011. Remote Sensing of Urban Surface Temperatures and the Surface Urban Heat Island.
- Voogt, J.A. and Grimmond, C. (2000) Modeling surface sensible heat flux using surface radiative temperatures in a simple urban area. *Journal of Applied Meteorology*, 39(10), 1679–1699.
- Voogt, J.A. and Oke, T. (1998) Effects of urban surface geometry on remotely-sensed surface temperature. *International Journal of Remote Sensing*, 19(5), 895–920.
- Voogt, J.A. and Oke, T.R. (1997) Complete urban surface temperatures. *Journal of Applied Meteorology*, 36(9), 1117–1132.
- Voogt, J.A. and Oke, T.R. (2003) Thermal remote sensing of urban climates. *Remote Sensing of Environment*, 86(3), 370–384.
- Wang, D. and Chen, Y., 2019. A Geometric Model to Simulate Urban Thermal Anisotropy in Simplified Dense Neighborhoods (GUTA-Dense). *IEEE Transactions on Geoscience and Remote Sensing*; 1–14.
- Wang, D., Chen, Y., Voogt, J.A., Krayenhoff, E.S., Wang, J. and Wang, L. (2020) An advanced geometric model to simulate thermal anisotropy time-series for simplified urban neighborhoods (GUTA-T). *Remote Sensing of Environment*, 237, 111547.
- Wang, D., Chen, Y. and Zhan, W. (2018) A geometric model to simulate thermal anisotropy over a sparse urban surface (GUTA-sparse). *Remote Sensing of Environment*, 209, 263–274.
- Weng, Q., Lu, D. and Schubring, J. (2004) Estimation of land surface temperature–vegetation abundance relationship for urban heat Island studies. *Remote Sensing of Environment*, 89(4), 467–483.
- Yang, J., Menenti, M., Krayenhoff, E.S., Wu, Z., Shi, Q. and Ouyang, X. (2019) Parameterization of urban sensible heat flux from remotely sensed surface temperature: effects of surface structure. *Remote Sensing*, 11(11), 1347.
- Yang, J., Wong, M.S., Ho, H.C., Krayenhoff, E.S., Chan, P.W., Abbas, S. and Menenti, M. (2020a) A semi-empirical method for estimating complete surface temperature from radiometric surface temperature, a study in Hong Kong city. *Remote Sensing of Environment*, 237, 111540.
- Yang, J., Wong, M.S. and Menenti, M. (2016a) Effects of urban geometry on turbulent fluxes: a remote sensing perspective. *IEEE Geoscience and Remote Sensing Letters*, 13(12), 1767–1771.
- Yang, J., Wong, M.S., Menenti, M. and Nichol, J. (2015) Study of the geometry effect on land surface temperature retrieval in urban environment. *ISPRS Journal of Photogrammetry and Remote Sensing*, 109, 77–87.
- Yang, J., Wong, M.S., Menenti, M., Nichol, J., Voogt, J., Krayenhoff, E.S. and Chan, P.W. (2016b) Development of an improved urban emissivity model based on sky view factor for retrieving effective emissivity and surface temperature over urban areas. *ISPRS Journal of Photogrammetry and Remote Sensing*, 122, 30–40.
- Yang, Z., Chen, Y., Zheng, Z., Huang, Q. and Wu, Z. (2020b) Application of building geometry indexes to assess the correlation between buildings and air temperature. *Building and Environment*, 167, 106477.
- Yao, R., Wang, L., Huang, X., Gong, W. and Xia, X. (2019) Greening in rural areas increases the surface urban heat island intensity. *Geophysical Research Letters*, 46, 2204–2212.
- Yu, K., Chen, Y., Wang, D., Chen, Z., Gong, A. and Li, J. (2019) Study of the seasonal effect of building shadows on urban land surface temperatures based on remote sensing data. *Remote Sensing*, 11(5), 497.
- Yuan, F. and Bauer, M.E. (2007) Comparison of impervious surface area and normalized difference vegetation index as indicators of surface urban heat Island effects in Landsat imagery. *Remote Sensing of Environment*, 106(3), 375–386.
- Zhan, W., Chen, Y., Voogt, J.A., Zhou, J., Wang, J., Ma, W. and Liu, W. (2012) Assessment of thermal anisotropy on remote estimation of urban thermal inertia. *Remote Sensing of Environment*, 123, 12–24.
- Zhou, B., Kaplan, S., Peeters, A., Kloog, I. and Erell, E. (2019) “Surface,” “satellite,” or “simulation”: mapping intra-urban microclimate variability in a desert city. *International Journal of Climatology*, 40(6), 3099–3117.
- Zhou, D., Xiao, J., Bonafoni, S., Berger, C., Deilami, K., Zhou, Y., Froliking, S., Yao, R., Qiao, Z. and Sobrino, J.A. (2018) Satellite remote sensing of surface urban Heat Islands: Progress, challenges, and perspectives. *Remote Sensing*, 11(1), 48.

How to cite this article: Yang J, Menenti M, Wu Z, et al. Assessing the impact of urban geometry on surface urban heat island using complete and nadir temperatures. *Int J Climatol*. 2021;41 (Suppl. 1):E3219–E3238. <https://doi.org/10.1002/joc.6919>